Title

Coupled analysis of unsteady aerodynamics and vehicle motion of a road vehicle in windy conditions

Author names and affiliations

Takuji Nakashima[a]*, Makoto Tsubokura[b,c], Mariano Vázquez[d,e], Herbert Owen[d], Yasuaki Doi[a]

[a] Department of Energy and Environmental Engineering, Faculty of Engineering, Hiroshima University
Address : 1-4-1 Kagamiyama, Higashi-Hiroshima, Hiroshima 7398527, Japan.
e-mails : nakashima@hiroshima-u.ac.jp, doi@naoe.hiroshima-u.ac.jp

[b] Division of Mechanical and Space Engineering, Faculty of Engineering, Hokkaido University
Address : Kita 13, Nishi 8, Kita-ku, Sapporo, Hokkaido 0608628, Japan
e-mail : mtsubo@eng.hokudai.ac.jp

[c] RIKEN Advanced Institute for Computational Science
Address : Kobe, Hyogo, Japan

[d] Department of Computer Applications in Science and Engineering, Barcelona Supercomputing Center
Address : Nexus I, Planta 2, C/GRAN CAPITA, 2-4, Barcelona 08034, Spain.
e-mails : mariano.vazquez@bsc.es, herbert.owen@bsc.es

[e] Artificial Intelligence Research Institute, Spanish National Research Council (IIIA-CSIC)
Address : Bellaterra, Barcelona, Spain.

*** Corresponding author**

Name : Takuji Nakashima
Affiriation : Department of Energy and Environmental Engineering, Faculty of Engineering, Hiroshima University
Address : 1-4-1 Kagamiyama, Higashi-Hiroshima, Hiroshima 7398527, Japan.
e-mail : nakashima@hiroshima-u.ac.jp
Phone : +81-82-424-7771
Fax : +81-82-424-7771

Abstract

The two-way coupling of full-scale vehicle motion and the surrounding turbulence motion has been realized on a developed unsteady aerodynamic simulator for a road vehicle. A large-eddy simulation (LES) technique has been applied to reproduce the unsteady turbulence motion, and an unstructured finite volume method has been adopted to explain the complicated geometry of a full-scale road vehicle. Three-degree-of-freedom equations of the vehicle's dynamic motion are incorporated into the developed LES code, and the motion is numerically reproduced by coupling the arbitrary Lagrangian–Eulerian (ALE) method and Navier–Stokes equations in a non-inertial reference frame. The simulation code is

implemented on a massively parallel processor to meet the demands of the large-scale, long-term aerodynamic simulations of full-scale road vehicles. As a typical application of the coupled analysis, an unsteady aerodynamics simulation of a simplified heavy-duty truck in windy conditions is demonstrated, and the effects of the unsteady aerodynamics on the truck's motion are investigated. The obtained results are compared with the results of a conventional quasi-steady analysis, and certain differences in the vehicle path and the yaw angle are identified. The effects of the transitional aerodynamics on variables related to driver's perception are significant. These results clearly indicate the importance of estimating the unsteady aerodynamic forces in a vehicle motion analysis.

Keywords: Large-eddy simulation, Vehicle aerodynamics, Coupled analysis.

1. Introduction

In the vehicle development process, the aerodynamic performance of a vehicle is evaluated using a steady or quasi-steady analysis. However, considerable attention needs to be paid to the unsteady aerodynamic effects on vehicles. Some of the typical cases in which the understanding of unsteady aerodynamics is crucial are as follows: the effects of atmospheric turbulence on the aerodynamic drag, running stability under gusty crosswind conditions, and driving stability in a high-speed condition. In all cases, the problem that we face is strongly related to the correlation between the ideal steady measurement in a wind tunnel and the real unsteady condition on the road.

In the past four decades, a number of experimental studies on the running stability of a vehicle under a gusty crosswind condition have been conducted [1-3]. In the previous literature, a significant overshoot of the yaw moment has been reported when the vehicle is subjected to a gusty crosswind. However, the effects of such unsteady aerodynamics on the vehicle's direct motion, particularly with respect to its safety, have not yet been thoroughly and quantitatively clarified. In fact, in the current analyses of vehicle motion [4], the aerodynamic forces included in the vehicle's motion equations are

still considered quasi-steadily because of the fact that the estimation of the unsteady aerodynamics by wind-tunnel measurements or on-road tests is fundamentally difficult. A large-eddy simulation (LES) is a promising candidate for the estimation of the transient aerodynamic forces acting on a vehicle [5].

Hence, we have developed a numerical method based on LES for estimating the unsteady aerodynamics of a road vehicle and have applied this method to some cases in which conventional wind-tunnel or on-road measurements are difficult to use [6-8]. The computational code was based on an unstructured finite volume method in order to treat a full-scale road vehicle with very complicated geometry. Two moving boundary techniques, a sliding grid method applied in [6] and an arbitrary Lagrangian–Eulerian (ALE) method [9] applied in [8], were integrated into the code in order to consider the vehicle's motion.

In this study, the developed numerical method has been extended by coupling it with three-degree-of-freedom equations of the vehicle's dynamic motion and a driver's reaction model, in order to consider the interactions between the vehicle motion and the vehicle aerodynamics. As an additional moving boundary technique to represent the large displacement caused by the translational motion of the vehicle, Navier–Stokes equations in a non-inertial reference frame was incorporated into the proposed method. This method was used in combination with the ALE method, which was applied for estimating the rotational motion. The coupled analysis of a full-scale vehicle required not only large-scale computational grids for representing the vehicle's complicated geometry but also long-term aerodynamic simulations for considering a time scale of the vehicle motion that was longer than the time scale of the turbulence around the vehicle. To satisfy the demands of such a high computational cost, the computational code was optimized for a massively parallel processor.

As an application of the developed numerical method, the coupled analysis of unsteady aerodynamics and vehicle motion [10] has been demonstrated in the case when a heavy-duty truck is subjected to sudden crosswind and the truck subsequently changes its pathway because of the transient aerodynamic forces acting on it. To identify the effects of unsteady aerodynamics on the vehicle motion,

the fully coupled simulation results have been compared with the results obtained by using conventional quasi-steady aerodynamics. Finally, the effects and the importance of the unsteady aerodynamics in the sudden crosswind condition have been discussed.

Nomenclature

A angle of the steering wheel (rad.).

C equivalent damping coefficient of a steering system (N m s/rad).

C_p pressure coefficient (-).

C_{Sm} model coefficient of Smagorinsky model for SGS turbulence model (-).

C_S lateral force coefficient of the vehicle (-).

C_{ym} yawing moment coefficient of the vehicle (-).

l_f, l_m, l_r distances from the center of gravity to the front, middle, and rear axles of the vehicle (m), respectively.

d_f, d_m, d_r wheel tracks of the front, middle, and rear axles of the vehicle (m), respectively.

f_d damping factor to represent the turbulent effect damping near a wall boundary.

F_d steering force of a driver (N).

Fx_{ij}, Fy_{ij} tire forces (N) in the longitudinal and lateral directions of the tire.

Fx'_{ij}, Fy'_{ij} tire forces (N) in the longitudinal and lateral directions of the vehicle.

$F_{w,x}$, $F_{w,y}$ aerodynamic longitudinal and lateral forces acting on the vehicle (N), respectively.

f_{ri} inertial force on a non-inertial reference frame in the i-th direction (m/s^2).

H_r model constant of a driver's reaction model (N).

I equivalent inertia moment of the steering system (kg m^2/rad).

I_z yaw inertia moment of the vehicle around its gravity center (kg m^2).

K_{st} equivalent elastic coefficient of the steering system.

m mass of the vehicle (kg).

$M_{w,z}$ aerodynamic yaw moment acting on a vehicle (Nm).

n inverse of steering ratio (-).

p pressure (Pa).

r radius of the steering wheel (m).

S frontal area of the vehicle (m^2).

u_i flow velocity in the i-th direction (m/s).

u_{gi} grid deformation velocity of the ALE method in the i-th direction (m/s).

t time (s).

T_r time interval for a delay of human reaction (s).

$T_{SAT,ij}$ self-aligning torque of the tire (Nm).

U,V longitudinal and lateral velocities of the vehicle (m/s).

V_{CW} crosswind velocity (m/s).

$V_{CW,\max}$ maximum crosswind velocity (m/s).

V_R relative speed between the air and a vehicle (m/s).

x_i coordinates in the i-th direction on a non-inertial reference frame (m).

X,Y absolute coordinates of vehicle's gravity center (m).

y^+ wall distance (-).

β_w aerodynamic yaw angle (rad.)

δ steering angle of front wheels of the vehicle (rad.).

ν dynamic viscosity of the air (m^2/s).

ν_{SGS} sub-grid scale eddy viscosity (m^2/s).

Ψ yaw angle of the vehicle (rad.).

ε predictable course deviation (m).

τ predictable time (s).

Subscripts and superscripts

$_{ij}$ subscript *i* indicates the front, middle, and rear axles, and subscript *j* indicates the left and right tires. For example, Fx_{11} is the longitudinal force on a front left tire, and Fy_{32} is the lateral force on a rear right tire.

$\overline{f}$ (Over-bar) spatially filtered value of the variable *f*.

$\dot{f}$ (Over-dot) first-order time differential of the variable *f*.

$\ddot{f}$ (Over-two-dot) second-order time differential of the variable *f*.

2. Numerical methods

2.1. Target vehicle and situation

The target vehicle of the coupled analysis in the present study is a simplified truck model developed in our previous study [11]. This model is based on the geometry of a 25-ton-class real commercial truck; its details are simplified to reduce the computational cost of the coupled analysis. The dimensions of the target truck are 12.0 m (length) × 2.54 m (width) × and 3.75 m (height). The weight of the simplified truck is assumed to be 9000 kg under a no-load condition. The center of gravity and the yawing moment of the inertia of the truck are determined using a general weight balance of the same-class heavy-duty trucks, which was updated from our previous vehicle dynamics analyses [10, 12] for a more realistic simulation.

The vehicle is assumed to move straight ahead at a constant speed of 25.1 m/s; it is driven into and out of a crosswind region, and $V_{CW,max}$ is set to the same value as the vehicle speed. Accordingly, the relative yaw angle of the vehicle with respect to the incoming flow drastically changes from 0° to 45° and then returns to 0° when the vehicle exits the crosswind region. As a result of the unsteady aerodynamic forces caused by the crosswind, the vehicle drifts in the lateral direction and deviates from

the original path; then, the driver model attempts to return the vehicle to its original track. The length of the crosswind region is set to approximately 50 m, which is approximately four times the vehicle length. Figure 1 shows the overview of the simplified truck geometry and a schematic representation of the target situation.

2.2. Governing equations

The governing equations of both fluid dynamics and vehicle dynamics analyses are mentioned in this section. After the description of each analysis model, the coupling of the two analyses will be mentioned.

2.2.1. Governing equations of fluid dynamics analysis

The incompressible Newtonian fluid is assumed, and the governing equations of fluid motion are given by the spatially filtered continuity and Navier–Stokes equations. Because of the high-Reynolds-number turbulence around the vehicle, a relatively high-wave-number turbulence that is impossible to capture by the allocated numerical grids is expressed by the sub-grid-scale (SGS) stress. To treat the vehicle motion in the fluid dynamics analysis, two numerical methods are adopted. The vehicle's horizontal translation motion is expressed by the Navier–Stokes equations in a non-inertial reference frame fixed on the vehicle's center of gravity. Thus, the vehicle's lateral and longitudinal motions are implicitly treated through the inertial force appearing in the Navier–Stokes equations. On the other hand, the vehicle's yawing, pitching, rolling, and vertical translation motions are estimated on the basis of the deformation of the computational grid. We have adopted the arbitrary Lagrangian–Eulerian (ALE) method for this purpose. Figure 2 shows the definitions of a coordinate system for the fluid dynamics analysis. The origin of the coordinate system is fixed at the center of gravity of the vehicle. However,

the directions of the coordinate axes are not changed by the vehicle's yawing rotation. The directions x_1, x_2, and x_3 were defined as the longitudinal, lateral, and vertical directions of the vehicle on the straight pathway, respectively. The application of the SGS turbulent eddy viscosity model to the governing equations leads to the following:

$$\frac{\partial \overline{u}_i}{\partial x_i} = 0 \quad , \qquad (1)$$

$$\frac{\partial \overline{u}_i}{\partial t} + \frac{\partial}{\partial x_j}\left(\overline{u}_i - u_{g,i}\right)\overline{u}_j = -\frac{\partial \overline{P}}{\partial x_i} + 2\frac{\partial}{\partial x_j}\left(\nu + \nu_{SGS}\right)\overline{S}_{ij} - f_{r,i}\,, \qquad (2)$$

$$\overline{S}_{ij} = \frac{1}{2}\left(\frac{\partial \overline{u}_j}{\partial x_i} + \frac{\partial \overline{u}_i}{\partial x_j}\right), \qquad (3)$$

$$\overline{P} = \overline{p}/\rho + \left(\overline{u_i u_i} - \overline{u}_i \overline{u}_i\right)/3\,, \quad (4)$$

where $f_{r,i}$ is opposite in sign to the translational acceleration of the vehicle in the ith direction.

As the SGS turbulent model for ν_{SGS} in Eq.(2), the standard Smagorinsky model [13] is applied as follows:

$$\nu_{SGS} = \left(C_{Sm} f_d \Delta\right)^2 \sqrt{2\overline{S}_{ij}\overline{S}_{ij}}\,, \quad (5)$$

where Δ is estimated by the third root of its volume. C_{Sm} is set to be 0.15, which is a verified value in an external flow around a simplified scale-model of a vehicle [8]. f_d is explained by the Van Driest-type damping function as follows:

$$f_d = 1 - \exp\left(-y^+/26\right) \quad . \qquad (6)$$

2.2.2. Governing equations of vehicle dynamics analysis

To simplify the problem in the vehicle dynamics analysis, the vertical motion of the vehicle is restrained and the pitching and rolling motion around the rotational center are assumed to be balanced

statically. Figure 3 shows the definitions of a coordinate system for the vehicle dynamics analysis. As shown in Fig. 3 (a), the origin of the coordinate system is fixed at the center of gravity and the coordinate axes are defined by the longitudinal, lateral, and horizontal axes of the moving vehicle. A similar equation system is validated for the vehicle motion of a compact car by Maruyama and Yamazaki [4], although the present system has been extended for a vehicle with six tires.

Based on the abovementioned assumption, the governing equations of the vehicle dynamics analysis become the motion equations of the moving vehicle in the lateral, transversal, and yawing directions as indicated below:

$$m\left(\dot{U} - V\dot{\psi}\right) = \sum_{i,j} Fx'_{ij} + F_{w,x}\,, \qquad (7)$$

$$m\left(\dot{V} + U\dot{\psi}\right) = \sum_{i,j} Fy'_{ij} + F_{w,y}\,, \qquad (8)$$

$$\begin{aligned} I_z\ddot{\psi} = \sum_{i,j} T_{SAT,ij} &+ \left(Fy'_{11} + Fy'_{12}\right)l_f + \left(Fx'_{11} - Fx'_{12}\right)\frac{d_f}{2} \\ &- \left(Fy'_{21} + Fy'_{22}\right)l_m + \left(Fx'_{21} - Fx'_{22}\right)\frac{d_m}{2} \\ &- \left(Fy'_{31} + Fy'_{32}\right)l_r + \left(Fx'_{31} - Fx'_{32}\right)\frac{d_r}{2} + M_{w,z}\,. \end{aligned} \qquad (9)$$

The relations among tire forces and their directions are also shown in Fig. 3. As shown in Fig. 3 (b), Fx'_{1j} and Fy'_{1j} on the front tires can be calculated as $Fx'_{1j} = Fx_{1j}\cos\delta - Fy_{1j}\sin\delta$ and $Fy'_{1j} = Fx_{1j}\sin\delta + Fy_{1j}\cos\delta$, respectively. δ was calculated by the motion equation of the steering system with a driver's reaction model, which is described below. On the other hand, Fx'_{ij} and Fy'_{ij} on the middle and rear tires are equal to Fx_{ij} and Fy_{ij}, respectively.

In general, Fy_{ij} and $T_{SAT,ij}$ depend on the load on the tire and the slip angle between the directions of the vehicle motion and the tire. Fx_{ij} depends on the load and the speed ratio between the tire rotation and the vehicle motion. Considering these dependencies, a magic formula model [14] is adopted to estimate the tire forces and SAT. Its model coefficients are determined from the experimental database.

In order to consider the driver's control when the truck runs off the target course, the second-order predictable correction model proposed by Yoshimoto [15] is adopted to determine the steering action of the driver. In this model, the future position of the vehicle after τ seconds is predicted from its current position, velocity, and acceleration. The driver's reaction is considered to be a steering force F_d, which is proportional to the predictable course deviation ε with the proportionality factor H_r: $F_d = H_r\varepsilon$. Moreover, in order to represent a time delay in the human reaction, the reaction is assumed to be discrete [15], and the steering force is evaluated at intervals of T_r seconds.

The steering action of the driver affects the steering angle of the front tires through the rotational motion equation of a steering system given as follows:

$$nI\ddot{A} + nC\dot{A} + K_{st}(nA - \delta) = \frac{F_d r}{n} . \quad (10)$$

Finally, the steering angle of the front wheel is evaluated as follows:

$$\delta = \frac{2T_{SAT,1j}}{K_{st}} + nA . \quad (11)$$

The parameter values are listed in Table 1. Parameters H_r, τ, and T_r related to the driver's reaction were validated for a compact car in Maruyama and Yamazaki [4]. The parameters of the steering system are determined by up-scaling the parameters of a compact car in Maruyama and Yamazaki [4] to those of a heavy-duty truck. On the basis of the steering radius and the steering ratio generally used in the same-class heavy-duty trucks, the equivalent inertia moment and the equivalent damping coefficient are set to be 4.8 times the values of the compact car, and the equivalent elastic coefficient is twice that of the compact car. The evaluation of the driver's reaction begins when the course deviation ε becomes larger than 0.5 m.

2.2.3. Coupling of two analyses

For the coupled analysis of the fluid dynamics around the vehicle and the vehicle dynamics, the governing equations are coupled in a straightforward manner. Both analyses are conducted simultaneously, while the outputs are exchanged at every moment. The attitude, velocity, and acceleration of the vehicle are obtained from the vehicle dynamics analysis for the fluid dynamics analysis. The two moving boundary methods are used for reproducing the motion in the fluid dynamics analysis. Simultaneously, the aerodynamic drag force, side force, and yawing moment in Eqs. (7)–(9) are input from the fluid dynamics analysis into the vehicle dynamics analysis. All six aerodynamic components are also input into the estimation of the static balance to determine the load on the tires.

2.3. Computational conditions

2.3.1. Computational domain and boundary conditions

The computational domain is defined as a rectangular duct with the length, width, and height of 124.5 m, 126.0 m, and 32.0 m, respectively. The domain is shown in Fig. 4 along with the boundary conditions. The vehicle is mounted approximately 29 m downstream of the boundary plane in front of the vehicle.

A uniform main flow of -25.1 m/s is imposed at the main inlet, which represents the relative velocity of the surrounding air with respect to the vehicle moving forward in a straight line. Then, the stepwise velocity profile shown in Fig. 1 is imposed on the sidewall as a lateral velocity condition, which traverses downstream at the same speed as the main inlet to reproduce the gusty crosswind. The details of this numerical technique for the sudden crosswind conditions are given in our previous reports [11, 16]. Furthermore, both the longitudinal and the lateral flow velocities uniformly shift with the change in the vehicle's translational velocity because of the non-inertial reference frame approach.

On the surface of the vehicle body, the yawing rotation is considered to be the Dirichlet condition of the velocity, and a wall model based on a logarithmic law of a fully developed turbulent boundary layer is applied to estimate the wall friction. The top and the bottom boundaries of the domain are treated as a free-slip wall, and a boundary behind the vehicle is treated as a free-outlet boundary with a gradient-free condition.

2.3.2. Numerical schemes

The governing equations of the fluid dynamics analysis are spatially discretized by a vertex-centered unstructured finite volume method. The SMAC algorism is employed for the pressure–velocity coupling. A second-order central difference scheme is applied for obtaining the spatial derivative and blended with 5% convective flux of a first-order upwind scheme for obtaining the convective term in the conservation equation of momentum in order to avoid numerical oscillation. Further, a third-order upwind scheme with Venkatakrishnan's limiter is applied only to the front region of the truck in order to avoid an overshoot of the lateral velocity profile before the crosswind region comes into contact with the vehicle. The second-order Adams–Bashforth scheme is adopted for time integration, and the time interval is set at 5.0×10^{-5} s.

Figure 5 shows the computational grid of the present fluid dynamics analysis. The number of vertices is approximately 3.3 million, and the number of elements is approximately 18.7 million, which mainly consists of tetrahedral elements. The other hexahedral, prism, and pyramid elements are only allocated near the boundary of the domain. By reproducing the yawing rotation of the vehicle using the ALE method, we rotate the surface grids on the vehicle in the yawing direction around the center of gravity. In order to avoid the excessive distortion of grids, the surrounding grids are also deformed using a spring analogy method. The details of numerical treatments of the ALE method in the computational code are described in [8].

For the numerical integration of the governing equations of the vehicle dynamics analysis, we adopt the fourth-order Runge–Kutta method. The motion equation of a steering system is also numerically integrated by the same method. The discretized time period is 5.0×10^{-5} s, as in the aerodynamics analysis.

The numerical analyses of the fluid dynamics and the vehicle dynamics are simultaneously conducted with the same time interval of the discretizations, as previously described. Their outputs are explicitly exchanged with each other at every time step.

2.3.3. Initial condition

By preparing the initial condition of the coupled analysis, we conduct a preliminary fluid dynamics simulation in a steady state without crosswind. This simulation begins from the uniform pressure and velocity field and is terminated after 1.5 s when the turbulent flow field around the truck develops. The coupled analysis is started from this developed flow field.

2.3.4. Analysis software

Numerical simulations are conducted using the LES code FrontFlow/red-Aero. The base code FrontFlow/red was optimized for HPC [6], and its accuracy on the steady aerodynamics analysis of a road vehicle has already been discussed and validated in our previous studies [6, 11]. An aerodynamics analysis of the ASMO (Aerodynamicsches Studien Modell) vehicle model has been conducted on two different computational grids with different spatial resolutions, and the pressure distribution and its convergence has been quantitatively validated by a comparison with the experimental data [6]. In [6], insufficient grid resolution for boundary layer on the vehicle model did not cause significant distortion on the prediction of the mean pressure distribution. Its effect was restrictive in the pressure distribution

and it was only observed around a trailing edge of the vehicle body as a spatial pressure oscillation. The flow structures around a full-scale vehicle have also been validated by comparing total pressure distributions with a wind-tunnel measurement of a real sedan-type vehicle [6]. The steady aerodynamics analysis of a heavy-duty truck has also been validated using a real commercial truck [11], which was the origin of the simplified truck geometry. The grid resolution on the truck body was comparable to the present simulation, and the predicted aerodynamic drag force was validated by a full-scale wind-tunnel measurement with an error within 9% at some yaw angles from 0° to 10°. The main problem causing this quantitative error was an inaccurate prediction of the friction force acting on the truck body caused by the insufficient grid resolution for the boundary layer. However, in the present study, we focus on the unsteady aerodynamics mainly caused by the vortex shedding from the edge of the truck body, and the inaccurate prediction of the friction is not a critical problem. The unsteady pressure force is expected to be predicted without a significant distortion, as discussed in the ASMO model analysis [6].

2.4. Parallel optimization

The computational costs of the coupled analysis of unsteady aerodynamics and vehicle motion are higher than those of the general LES of vehicle aerodynamics in a steady state because the turbulent phenomena around a vehicle have a considerably shorter time scale than the vehicle motion, and hence, a significantly large number of time steps have to be simulated. In order to realize the coupled analysis, the code FrontFlow/red-Aero is optimized again for a relatively large-scale parallel computer in the present study.

2.4.1. Code optimization

The parallel optimizations of the code have been conducted on a parallel supercomputer MareNostrum (MN) in Barcelona Supercomputing Center. The code's performance is first analyzed by a performance analysis tool named Paraver. Then, the clarified shortcomings of the code are overcome by making two main modifications. One is an improvement of the load balance in the calculation using multi-type elements. The number of floating operations required in each type of element has been counted, and a domain decomposition process for parallel processing has been modified by considering the required number of operations for each element. The other modification is a reduction of the all-to-all communication in an iterative matrix solver for the pressure equation.

The parallel performance of the modified code is investigated using a benchmark problem, which is a typical aerodynamics analysis of the simple bluff-body on an unstructured grid with 3.3-million nodes and 14-million elements. The computational methods for the fluid dynamics analysis are almost the same as for the coupled analysis in the present study, except for the special treatments of the crosswind and vehicle motion. The number of iterations for the ICCG solver for the pressure equation is fixed at 200 for every time step. The calculation speed is estimated from the CPU time for a 100-time-step calculation.

The speed-up of the calculation on the parallel processor is shown in Fig. 6. The calculation speed is linearly accelerated up to 1024 cores on the MN, and the effect of the optimization is confirmed. The same benchmark is also conducted on SR11000 (SR) in the Information Technology Center at The University of Tokyo, and its result is also shown in Fig. 6. On this supercomputer, the calculation speed hits a peak at 512 cores. The possible cause of this degradation is the relatively high execution efficiency of SR, which can execute the benchmark calculation approximately 2.5 times faster than the MN when considering the case of 16 cores; this result may emphasize the overheads of the communication.

2.4.2. Modification of grid deformation process

Furthermore, the grid deformation process using a spring analogy in the ALE method is optimized for a large parallel processor. To reduce the computational and communication costs in the iterative solver for the spring analogy method, a key-frame technique is introduced. In this technique, the grid deformations at the typical attitude of the vehicle are calculated preliminarily; the displacements of the grid points, called key-frames, are stored for each process before the beginning of the coupled analysis. Then, in the coupled analysis, the instantaneous displacement of the grid points is linearly interpolated from the nearest two key-frames at every time step; no communication is necessary for this process.

2.4.3. Execution of coupled analysis

Finally, the coupled analysis is conducted on the 16 nodes/256 CPUs of the SR11000. The coupled simulation of the fluid and the vehicle dynamics for 10 s of physical time take approximately 100 h of wall-clock time.

3. Results and discussion

3.1. Steady aerodynamics analysis

Before conducting the coupled analysis, we conducted the steady aerodynamics analyses at various yaw angles. The yaw angle was set at every 5° from 0° to 45°. In these analyses, the velocities imposed on the front and side boundaries were constant and uniform for the steady yaw angle condition, and the other computational conditions, setups, and methods were the same as those of the coupled analysis.

The time-averaged aerodynamic coefficients in each condition are shown as points in the graphs of Fig. 7. Here, the aerodynamic side force and yaw moment coefficients could be expressed as

$$F_{w,y} = \frac{1}{2} C_S(\beta_w) \rho S V_R^2 \quad \text{and} \quad (12)$$

$$M_{w,z} = \frac{1}{2} C_{ym}(\beta_w) \rho S \left(l_f + \frac{l_m + l_r}{2} \right) V_R^2, \quad (13)$$

respectively.

Based on these results, the approximate polynomials of the aerodynamic coefficients in β_w are determined by the least-square method. The constructed approximate curves are also given in Fig. 7. The approximate polynomials are constructed not only for these two components but also for all six components; these polynomials are applied to estimate the aerodynamic forces and moments in the conventional vehicle dynamics analysis on the basis of the quasi-steady aerodynamics described below.

3.2. Aerodynamics in coupled analysis

Next, the coupled analysis of unsteady aerodynamics and vehicle motion is conducted. As a result of the fluid dynamics simulation in the coupled simulation, the time series of the aerodynamic yawing moment and the side force are shown in Fig. 8. The conventional vehicle dynamics analysis based on the steady aerodynamic database is also conducted under the same sudden crosswind condition in order to compare it with the coupled analysis and to clarify the effects of the unsteady aerodynamics. The results of the conventional analysis are also shown in the figures.

In the conventional analysis, the aerodynamic yaw angle β_w is calculated at every time step from the vehicle velocity and the crosswind velocity at the center of gravity of the truck, which is given by the profile shown in Fig. 1. The aerodynamic forces and moments are evaluated by using the approximated polynomial of the aerodynamic coefficients in the β_w calculated above. The evaluated forces and moment are input into the motion equations (7)–(9), and the vehicle's motion in the next time step is determined.

The yawing moments $M_{w,z}$ in Fig. 8 (a) exhibit considerably different behaviors in the two analyses. In the coupled analysis, in which the transient phenomena are considered, the yaw moment has high positive and negative peaks. These peaks are caused by the crosswind acting on the front half and the rear half of the truck as the truck is driven into and out of the crosswinds, respectively. On the other hand, in the conventional analysis with the quasi-steady aerodynamics evaluation, the yawing moment exhibits an almost monotonic decrease and increase because the crosswind velocity and the aerodynamic yaw angle are determined at the center of gravity and the crosswind effect appears only after the center of gravity of the truck is driven into the crosswind.

The lateral forces $F_{w,y}$ in Fig. 8 (b) exhibit a similar profile in the two analyses, although they show different gradients at the edges of the step. The force monotonically increases as the truck is driven into the crosswind region and decreases to zero as the truck exits the region. The differences in the gradients are also caused by transient aerodynamics. In the coupled analysis, the crosswind effect takes a longer time to reach the steady state than that in the conventional analysis because, in the former case, the crosswind first acts on the front part of the truck and then its effect gradually spreads to the tail part.

3.3. Flow field visualization

Figure 9 shows the snapshots of the pressure and lateral velocity fields around the truck. Here, the lateral velocity v_2 is not the velocity u_2 on the non-inertial reference frame but the velocity on a rest frame. Figure 10 shows the surface pressure on the lateral surface of the truck in the fully coupled simulation. Both figures give values at typical instances from t = 0.2 s to 4.0 s.

In the still air at t = 0.2 s, the pressure and velocity fields are almost symmetric, and the truck is on the straight path Y = 0, which is shown by the black dotted lines in the figures. At t = 0.88 s, when the yaw moment reaches the positive peak, the front half of the truck is subjected to the crosswind, which is

shown as a high lateral velocity. The asymmetric pressure distribution around the cabin appears although the separation on the leeward side is not enhanced at this moment. When the entire truck is subjected to the crosswind at t = 2.0 s, a large separation region appears on the leeward side and a fluctuating pressure distribution is observed on this side of the lateral surface. The high-pressure region on the windward side of the truck spreads widely on the container. At t = 2.87 s, when the yaw moment reaches the negative peak, the front half of the truck is exiting the crosswind. The pressure on the cabin recovers its symmetric property in spite of the fluctuating low pressure on the leeward side caused by the remaining separation of the flow. The high pressure on the windward side of the container also remains. Finally, at t = 4.0 s, the velocity field recovers its symmetrical property; the small asymmetric property remaining in the pressure fields is caused by the lateral motion of the vehicle.

3.4. Vehicle motion in coupled analysis

The time series of the lateral displacement and the yaw angle of the vehicle are plotted in Fig. 11. Here, the lateral displacement implies a course deviation because a straight path is assumed in this analysis. For reference, the results of the conventional analysis are also plotted. In the coupled analysis, the yaw of the vehicle begins to increase when it reaches the crosswind region around t = 1 s, and the vehicle begins to deviate from the original path. The lateral displacement continues to increase after the vehicle exits the crosswind region until t = 5 s, while the yaw angle has a value of around 4° until t = 4 s. The yaw angle drastically decreases because of the steering action of the driver.

A significant difference in the yaw angle between the quasi-steady analysis and the coupled simulation is identified. The difference in the initial response to the crosswind around t = 1 s is particularly remarkable. This difference is caused by the different behavior of $M_{w,z}$ shown in Fig. 8; the transient aerodynamics that appears as the positive peak of $M_{w,z}$ leads to the positive yaw angle in the

initial response. In contrast, the other typical transient aerodynamics represented by a negative peak of $M_{w,z}$ when the vehicle exits the crosswind, leads to a gradual gradient of the yaw angle around t = 3 s.

With regard to the lateral displacement, the maximum difference is observed to be 0.83 m at T = 3.2 s. As for the maximum displacements around t = 5.8 s, the quasi-steady analysis predicted a deviation 0.53-m larger than that in the coupled analysis. These differences in the yaw motion and lateral deviation indicate the effects of unsteady aerodynamics on vehicle motion, which are significant for a precise estimation of the trajectory of a vehicle subjected to a gusty crosswind.

In terms of the evaluations of the vehicle's running stability or drivability, the differences in the two analyses are also significant. The yaw rate $d\Psi/dt$ is one of the most famous index parameter for the evaluation of the stability and the drivability of a road vehicle in the field of automobile engineering. The amplitude of the steering wheel angles A is reported as a parameter strongly related to the driver's perception of the running stability in crosswinds [17]. The behaviors of these two variables are shown in Fig. 12. The yaw rates exhibit completely different behaviors between the two analyses when the vehicle is subjected to the crosswind. The maximum difference of the steering wheel angles is observed to be 35° at t = 2.2 s and 4.0 s. Its positive extremum in the coupled analysis is 2.5 times smaller than that in the quasi-steady analysis. These differences indicate the importance of the effects of unsteady aerodynamics on the evaluation of the stability and drivability of a vehicle subjected to a gusty crosswind.

4. Conclusions

In the present study, we developed an unsteady aerodynamic simulator of a road vehicle by accomplishing the fully coupled analysis of vehicle motion and the transient flow around the vehicle. In order to consider the vehicle's motion in the unsteady fluid dynamics analysis, the ALE method for the rotational motions and the non-inertial reference frame method for the translational motions were

introduced together. To realize the coupled analysis of a full-scale vehicle with a complicated geometry, it was necessary to conduct an LES analysis for a long period of time using large-scale computational grids. Therefore, the LES code was optimized for a massively parallel processor; the modified code achieved the linear acceleration of the computational speed of up to 1000 cores.

The developed unsteady aerodynamics simulator of a road vehicle was applied to the case when a heavy-duty truck was subjected to a sudden crosswind. The obtained results were compared with the results of a conventional quasi-steady analysis. We identified certain differences in the vehicle path and the yaw angle between the quasi-steady and the fully coupled analyses. The differences in the variables related to a driver's feeling were also significant. These results clearly indicated the importance of estimating the unsteady aerodynamic forces in a vehicle motion analysis.

Acknowledgments

We would like to express our sincere gratitude to Dr. K. Kitoh from Kitoh Kozo Technology, Inc. and Mr. Y. Sasaki from Numerical Flow Designing Co., Ltd. for their design of the simplified truck model. Further, we would like to thank Mr. T. Ikenaga and Mr. S. Matsuda from Hiroshima University for their support during the construction of the analysis system of vehicle dynamics. We also would like to express our sincere gratitude to Dr. G. Houzeaux and Dr. J. Gimenez from the Barcelona Supercomputing Center for their valuable support in the performance analysis and the parallel optimization of the computational code. This work is supported by the Industrial Technology Research Grant Program in 2007 from New Energy and Industrial Technology Development Organization (NEDO) of Japan. The analysis software FrontFlow/red-Aero used in this study is based on a software FrontFlow/red developed in Revolutionary Simulation Software (RSS21) sponsored by the Ministry of Education, Culture, Sports, Science and Technology, Japan. A part of this work is also supported by the

Institutional Program for Young Researcher Overseas Visits from Japan Society for the Promotion of Science (JSPS).

References

[1] Beauvais F N. Transient nature of wind gust effect on an automobile. SAE Paper 1967. No.67068.

[2] Kobayashi T, Kitoh K. Cross-wind effects and the dynamics of light cars. Int J Vehicle Design 1983; Special Publication SP3: 142-157.

[3] Dominy R G, Ryan A. An improved wind tunnel configuration for the investigation of aerodynamic cross wind gust response. SAE Paper 1999. No.1999-01-0808.

[4] Maruyama Y, Yamazaki F. Driving simulator experiment on the moving stability of an automobile under strong crosswind. J Wind Eng Ind Aerod 2006;94:191-205.

[5] Hemida H, Krajnovic S. Transient simulation of the aerodynamic response of a double-deck bus in gusty winds. J Fluids Eng Trans ASME 2009;131:031101-1-10.

[6] Tsubokura M, Kobayashi T, Nakashima T, Nouzawa T, Nakamura T, Zhang H, Onishi K, Oshima N. Computational visualization of unsteady flow around vehicles using high performance computing. Computers & Fluids 2009;38:981-990.

[7] Tsubokura M, Nakashima T, Kitayama M, Ikawa Y, Doh D H, Kobayashi T. Large eddy simulation on the unsteady aerodynamic response of a road vehicle in transient crosswinds. Int J Heat Fluid Flow 2010;31:1075-1086.

[8] Cheng S, Tsubokura M, Nakashima T, Nouzawa T, Okada Y. A numerical analysis of transient flow past road vehicles subjected to pitching oscillation. J Wind Eng Ind Aerod 2011;99:511-522.

[9] Hirt C W, Amsden A A, Cook J L. An arbitrary Lagrangian-Eulerian computing method for all flow speeds. J Comp Phys 1974;14:227-253.

[10] Nakashima, T., Tsubokura, M., Ikenaga, T., Kitoh, K., and Doi, Y. Coupled Analysis of Unsteady Aerodynamics and Vehicle Motion of a Heavy Duty Truck in Wind Gusts. Proceedings of ASME 2010 3rd Joint US-European Fluids Engineering Summer Meeting: Volume 1, Symposia – Parts A, B, and C. Paper no. FEDSM-ICNMM2010-30646:2659-2668.

[11] Tsubokura M, Takahashi K, Matsuuki T, Nakashima T, Ikenaga T. HPC-LES for unsteady aerodynamics of a heavy duty truck in wind gust 1st report: Validation and unsteady flow structures. SAE Paper 2010. No.2010-01-1010.

[12] Nakashima T, Ikenaga T, Tsubokura M, Doi Y. HPC-LES for unsteady aerodynamics of a heavy duty truck in wind gust 2nd report: Coupled analysis with vehicle motion. SAE Paper 2010. No. 2010-01-1021.

[13] Smagorinsky J. General circulation experiments with the primitive equations, I. The basic experiment. Monthly Weather Rev 1963;91:99-164

[14] Bakker E, Pacejka H B, Linder L. A new tire model with an application in vehicle dynamics studies. SAE Paper 1989. No. 890087.

[15] Yoshimoto K. Simulation of driver-vehicle systems using a predictable model of driver's steering. J Japan Society of Mechanical Engineers 1968;71:1181-1186. (in Japanese)

[16] Ikenaga T, Nakashima T, Tsubokura M, Kitoh K, Doi Y. Large-eddy simulation of a vehicle driving into crosswind. Rev Automot Eng 2009;31:71-76.

[17] Maeda K, Sakai H. Aerodynamic effects on stability at a high-speed running vehicle in the crosswind. J Soc Automot Eng Jpn 1994;48:54-59. (in Japanese)

Table and Figures

Table 1. Parameters of the steering system and human reaction model

Parameter	Value	Unit
Mechanical		
r	0.24	m
n	0.032	-
I	5.7×10^{1}	kg m^2
C	4.2×10^{3}	N s
K_{st}	9.7×10^{4}	N
Human		
H_r	3.9	N/m
τ	2.0	s
T	0.60	s

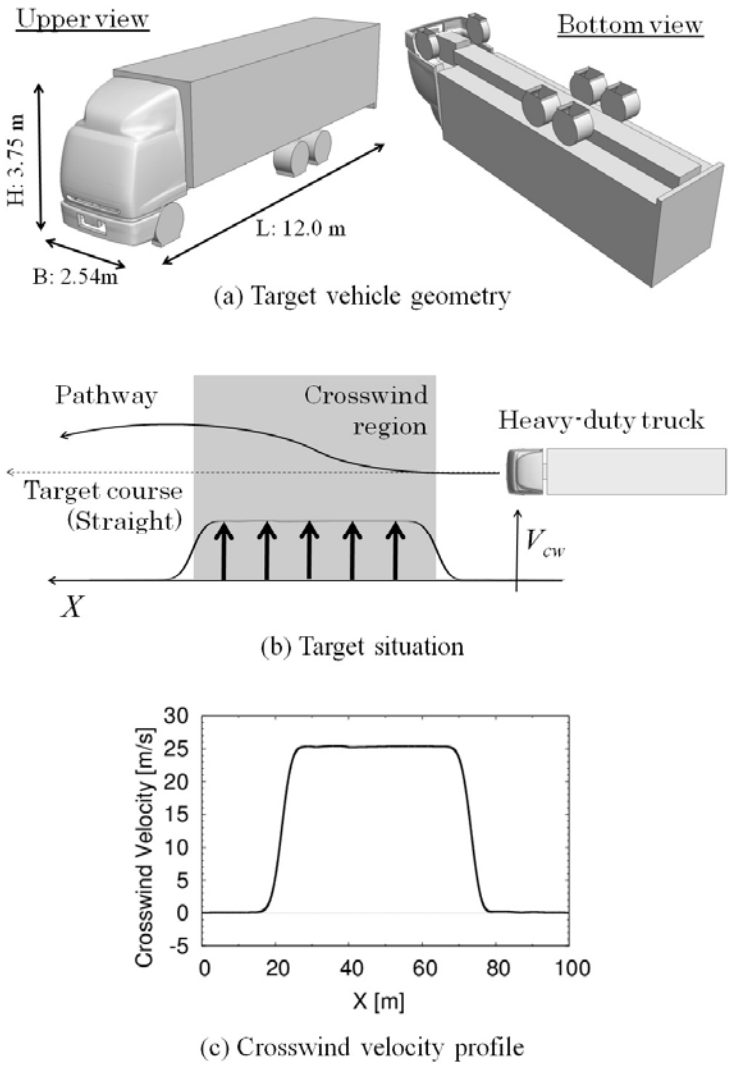

Fig. 1 Overview of the geometry of the target heavy-duty truck and the target situation of sudden crosswind

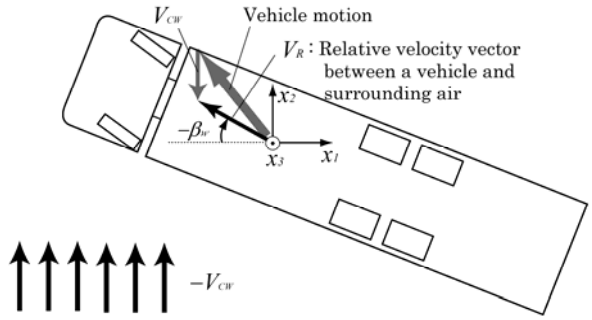

Fig. 2 Definition of coordinate system and variables for fluid dynamics simulation.

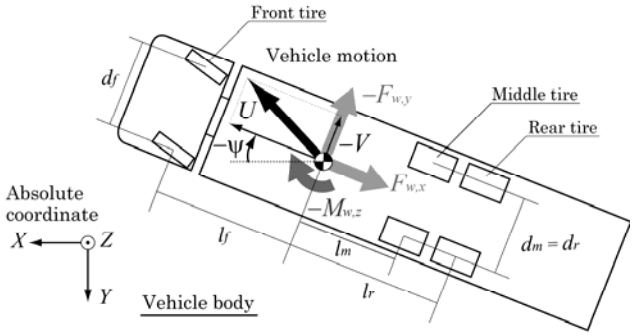

(a) vehicle body

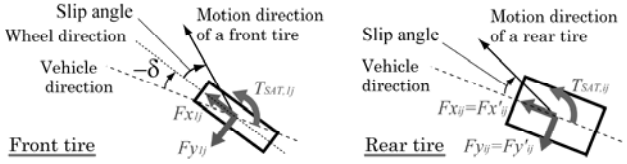

(b) tires

Fig. 3 Definition of coordinate system and variables for vehicle dynamics simulation.

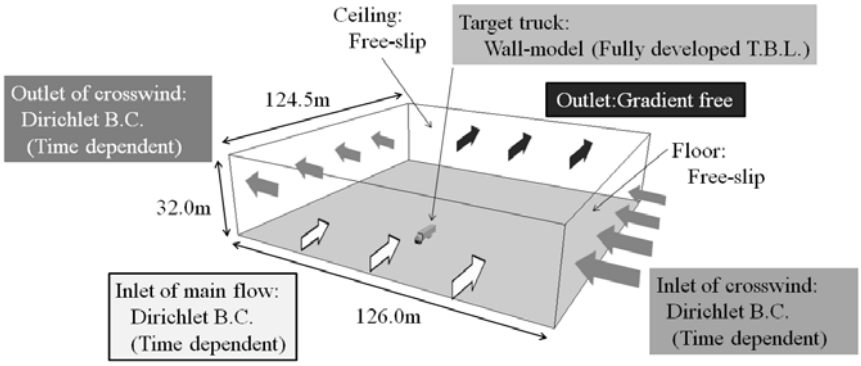

Fig. 4 Computational domain

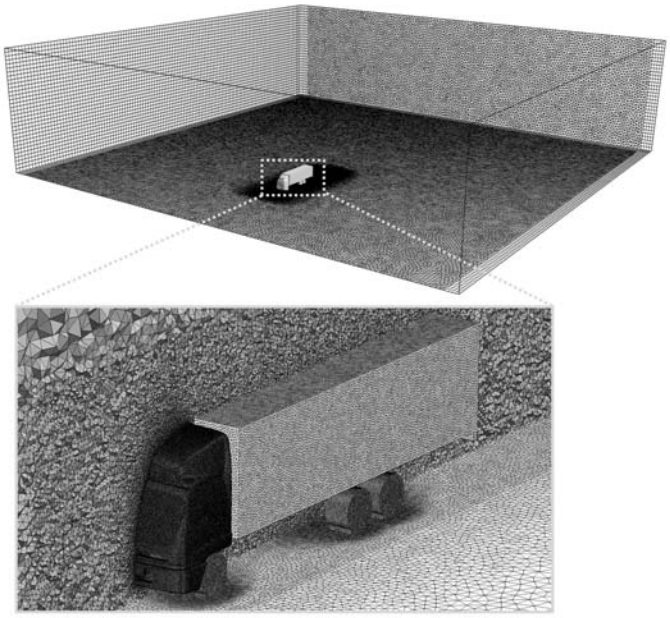

Fig. 5 Computational grids on boundary surfaces

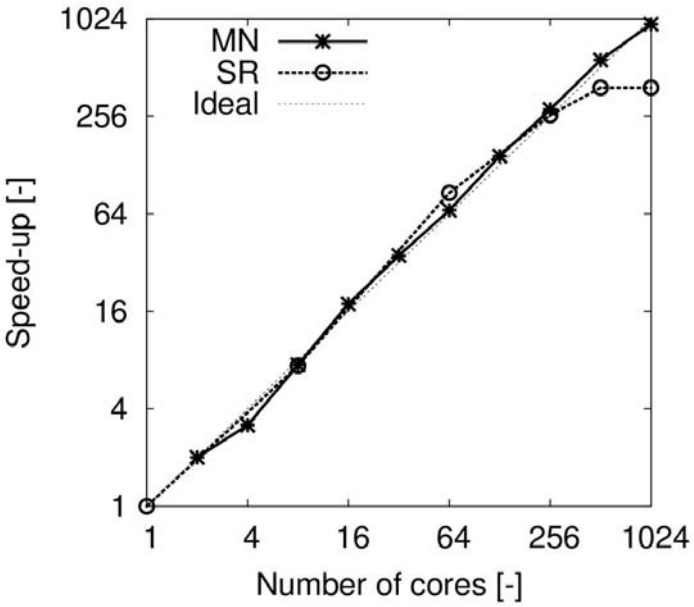

Fig. 6 Parallel performance of the numerical code

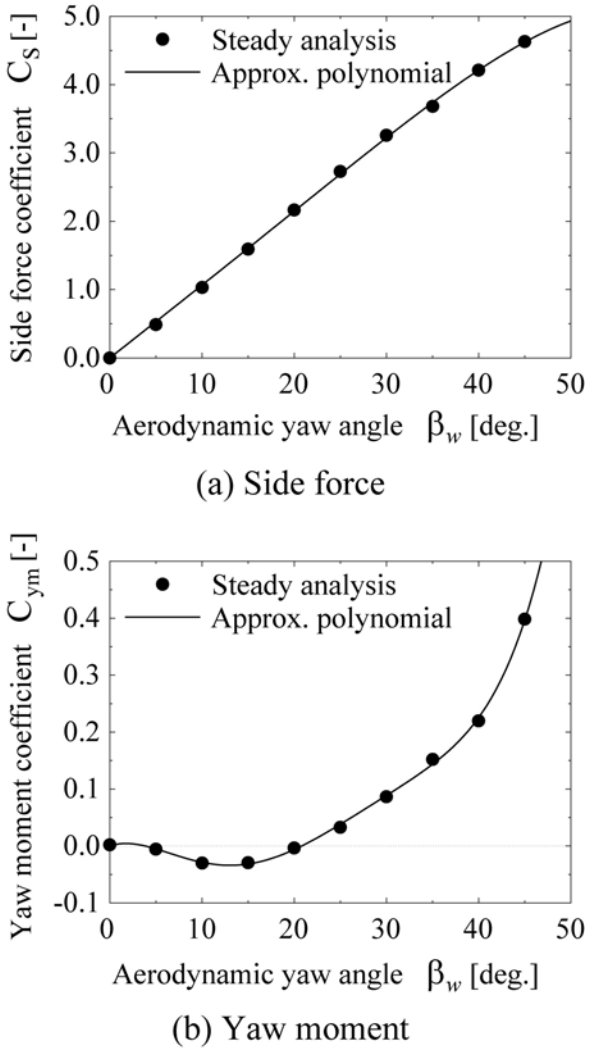

Fig. 7 Quasi-steady aerodynamic coefficients C_S and C_{ym} and their approximate polynomials

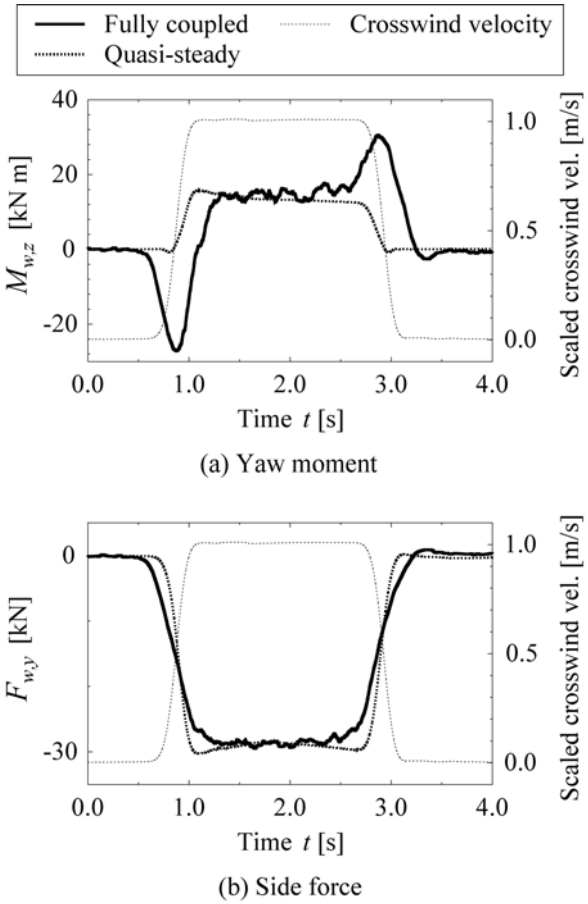

Fig. 8 Time-series of aerodynamic yaw moment $M_{w,z}$ and side force $F_{w,y}$ acting on the truck

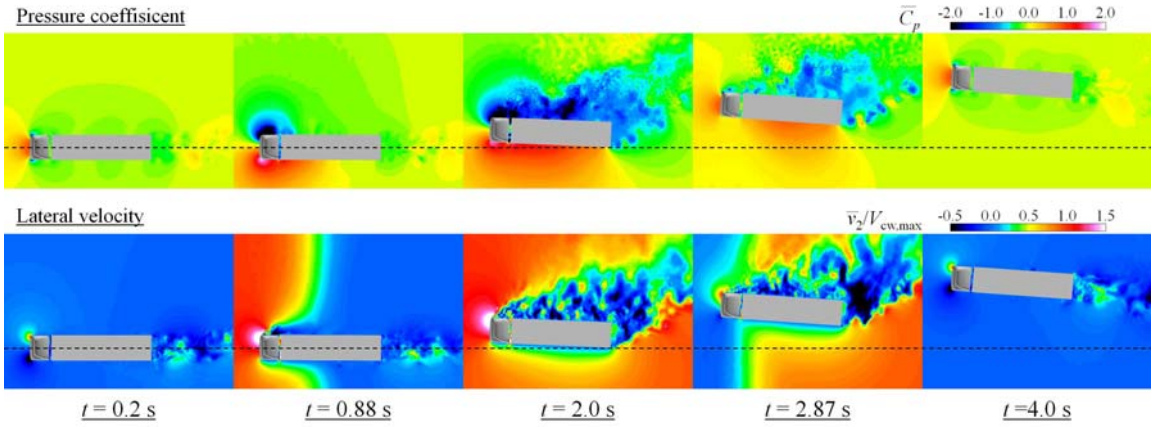

Fig. 9 Snapshots of the pressure coefficient C_p (top) and the spanwise velocity u_2 (bottom) distributions at the half height of the vehicle.

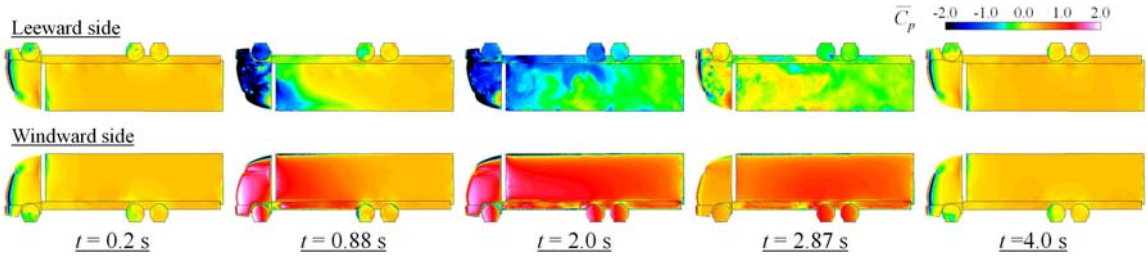

Fig. 10 Snapshots of the pressure coefficient C_p distribution on the lateral surface of the truck. (Top: leeward side. Bottom: windward side.)

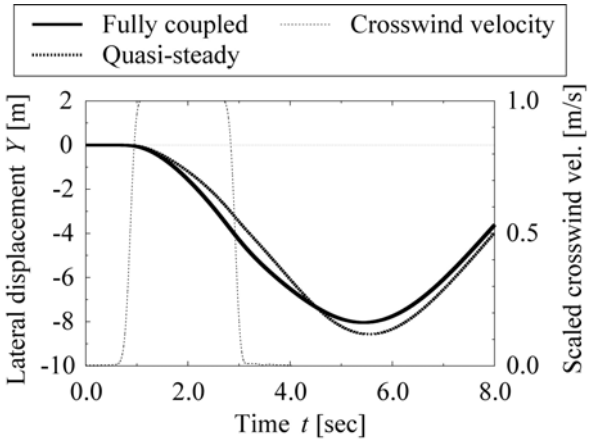

(a) Lateral displacement

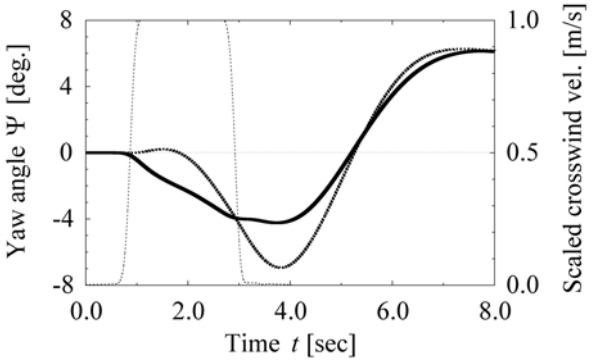

(b) Yaw angle

Fig. 11 Time series of the lateral course deviations (top) and yaw angles (bottom).

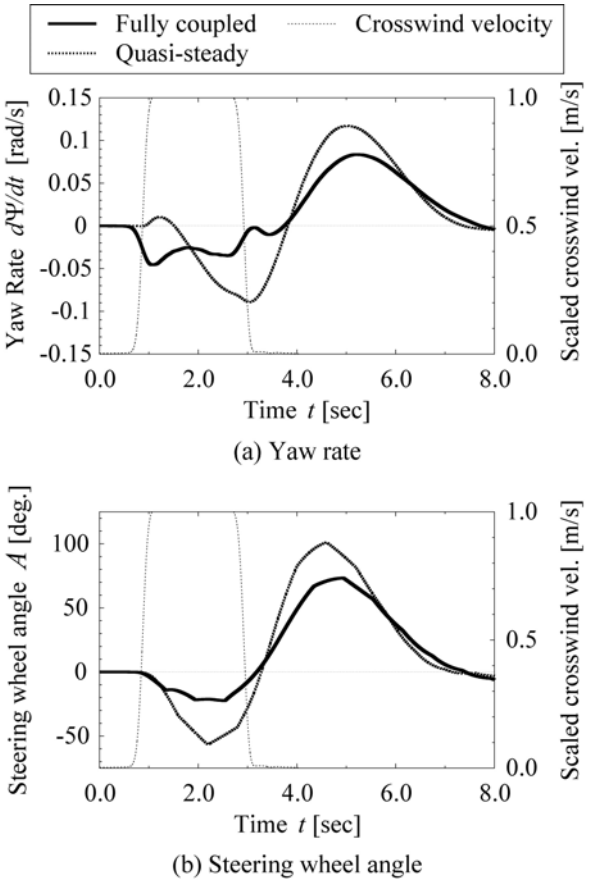

Fig. 12 Time series of the yaw rate of the truck (top) and the steering wheel angle (bottom).